Hindawi
Journal of Chemistry
Volume 2019, Article ID 9742826, 7 pages
https://doi.org/10.1155/2019/9742826

Research Article

An Initial Evaluation on the Adsorption of SO_2 and NO_2 over Porous Fe_3O_4 Nanoparticles Synthesized by Facile Scalable Method

Xuan-Manh Pham,[1] **Duy Linh Pham**,[1] **Nguyen Thi Hanh**,[1,2] **Tuyet Anh Dang Thi**,[1,2] **Le Nhat Thuy Giang**,[1,2] **Hoang Thi Phuong**,[1] **Nguyen Tuan Anh**,[1] **Hac Thi Nhung**,[1,2] **Giang Truong Le**,[1] **Mai Ha Hoang**,[1,2] **and Tuyen Van Nguyen**[1,2]

[1]*Institute of Chemistry, Vietnam Academy of Science and Technology, 18 Hoang Quoc Viet, Cau Giay, Hanoi, Vietnam*
[2]*Graduate University of Science and Technology, Vietnam Academy of Science and Technology, 18 Hoang Quoc Viet, Cau Giay, Hanoi, Vietnam*

Correspondence should be addressed to Mai Ha Hoang; hoangmaiha@ich.vast.vn and Tuyen Van Nguyen; ngvtuyen@hotmail.com

Received 13 March 2019; Revised 24 April 2019; Accepted 9 May 2019; Published 12 June 2019

Guest Editor: Van Duong Dao

In this study, Fe_3O_4 nanoparticles used as an adsorbent for the removal of toxic gases were successfully synthesized via the facile coprecipitation method. The Fe_3O_4 nanoparticles displayed a well-defined morphology with the size of ~10 nm and a porous structure with a specific area of 115.90 m^2/g and a wide range of pore sizes. These nanoparticles exhibited effective adsorption abilities upon the exposure to toxic gases. In particular, the amount of 40.5 mg SO_2 and 108.5 mg NO_2 was adsorbed in 1 g of Fe_3O_4 nanoparticles after 60 minutes of exposure, making the Fe_3O_4 nanoparticles become a promising adsorbent for the removal of toxic gases.

1. Introduction

Toxic gases that are present during the fires are one of the main causes of fire deaths [1]. Depending on the materials that are burning, some kind of different toxic gases might be produced. These gases may include carbon monoxide (CO), nitrogen dioxide (NO_2), sulfur dioxide (SO_2), and hydrogen cyanide (HCN) [2]. They prevent cellular respiration, leading these cells to death or causing irritation, and are toxic for the body, at a higher level causing death quickly [3]. In addition to carbon monoxide, the main agent of deaths in the fire, nitrogen dioxide and sulfur dioxide are also known as dangerous agents for the humans' life. Hence, the removal of these gases from the fire is necessary to protect humans. Nanoparticle powders with a large specific surface area have been proposed for adsorption and cleaning up of fumes and toxic gases generated in fires [4]. The hydroxide, carbonate, bicarbonate, and oxides of metal have attracted wide attention for that because they can be decomposed to CO_2 and H_2O to extinguish the fire or can be resistant to the fire flame improving the isolating ability of flammable materials with fire and oxygen [5–8]. Among them, the Fe_3O_4 nanostructured material is a potential candidate due to its stability, high surface area, and easy synthesis [9]. Some researchers have pointed out that Fe_3O_4 can be an efficient adsorbent for the removal of heavy metal ions [9–11] and inorganic anions [12] from aqueous solutions. However, there have been very few reports using Fe_3O_4 as an adsorbent for the removal of nitrogen dioxide and sulfur dioxide.

The removal of SO_2 and NO_2 has been also investigated in the field of environment because the amount of these gases released in atmosphere can induce acid rain which is harmful to humans [13, 14]. Active carbon has been known as an effective adsorbent in processes of removing stack

gases [15]. Nevertheless, it is difficult to apply active carbon for the removal of SO_2 and NO_2 in fires due to its flammable nature.

In this work, Fe_3O_4 nanoparticles were prepared by a facile scalable method and applied as an adsorbent for the adsorption of NO_2 and SO_2. The material was characterized by a number of analytical techniques. The Fe_3O_4 nanoparticles exhibited good adsorption abilities in the removal of SO_2 and NO_2.

2. Experimental Section

2.1. Synthesis of Fe_3O_4 Nanoparticles. All chemicals were of analytical grade. Iron(III) chloride hexahydrate ($FeCl_3{\cdot}6H_2O$), iron(II) chloride tetrahydrate ($FeCl_2{\cdot}4H_2O$), ammonia solution 25% ($NH_3{\cdot}H_2O$), sulfur dioxide (99.9%), nitrogen dioxide (99.5%), and nitrogen (99.999%) were purchased from Sigma-Aldrich and used without any further purification. The magnetite (Fe_3O_4) nanoparticles were prepared by the following coprecipitation method [16–18].

In brief, $FeCl_3{\cdot}6H_2O$ (0.05 mol, 13.52 g) and $FeCl_2{\cdot}4H_2O$ (0.03 mol, 5.96 g) were dissolved in 100 mL DI water with a Fe^{2+}/Fe^{3+} molar ratio of 0.6. Then, the ammonium solution was added dropwise into the solution until pH = 11.0 over a period of 2 h, under vigorous stirring to achieve Fe_3O_4 nanoparticles with high purity. The obtained precipitate was filtered, washed with DI water, and dried in vacuum at 60°C for 24 h.

2.2. Material Characterization. The specific surface area was determined from N_2 adsorption/desorption at 77 K by the Brunauer–Emmett–Teller (BET) method using a Micrometrics surface area analyzer (TriStar II Plus, Micromeritics Instrument Corp, USA). The morphology and particle size were determined by field emission scanning electron microscope (FE-SEM, S-4800, Hitachi, Japan) and particle-size distribution measurement (Litesizer™ 500, Anton Paar Instrument Co. Ltd., Austria). The structure of adsorbents was characterized by high-resolution XRD (D/max Ultima III, Rigaku, Japan). The thermogravimetric analysis (TGA) was determined on TGA-50, Shimadzu, Japan, in an air atmosphere with a heating rate of 5°C·min^{-1} from room temperature to 700°C. Temperature-programmed reduction (TPR) was carried out under 5% CO in Ar flow (100 cc/min) at a heating rate of 10°C/min, from room temperature to about 900°C using AutoChem™ II 2920 (Micromeritics Instrument Corp, USA).

2.3. Adsorption Experiments. For the adsorption study, 1 g of Fe_3O_4 nanoparticles were exposed to dried SO_2 and NO_2 at a particular time in the fixed bed reactor under ambient temperature. These gases were mixed with nitrogen as a carrier gas (5% SO_2 or NO_2 in the N_2 atmosphere). The Fe_3O_4 nanoparticles were pretreated under an Ar flow at 400°C during 2 h and then cooled to the room temperature. After that, the gas stream was supplied with a flow rate of 200 cc/min. The uptake quantities were recorded as a function of time based on a mass change of samples. The presence of the gas phase in contact with the materials was monitored by the FTIR measurement (Thermo Fisher, USA) at 8 cm^{-1} resolution. In addition, energy-dispersive X-ray spectroscopy (SEM-EDX) (HORIBA-EMAX80; Hitachi High-Technology) was used to evaluate the presence as well as the adsorbed quantity of SO_2 and NO_2.

3. Results and Discussion

3.1. Characterization of Fe_3O_4 Nanoparticles. The porous, interconnected Fe_3O_4 nanoparticles were synthesized using a facile scalable method. The mixture solution of $FeCl_3$ and $FeCl_2$ was prepared with a Fe^{2+}/Fe^{3+} molar ratio of 0.6. The used Fe^{2+}/Fe^{3+} molar ratio is higher than the Fe^{2+}/Fe^{3+} molar ratio in Fe_3O_4 because a part of Fe^{2+} oxidized to Fe^{3+} will lead to the lower Fe^{2+}/Fe^{3+} molar ratio. The increase of Fe^{2+} concentration can attain the ideal Fe^{2+}/Fe^{3+} molar ratio of ~0.5. Then, the ammonium solution was added dropwise into the solution until pH = 11.0 to achieve Fe_3O_4 nanoparticles with high purity. Figure 1 shows the X-ray diffraction (XRD) patterns of the synthesized Fe_3O_4. All peaks were indexed to cubic Fe_3O_4 (JCPDS: 01-088-0315) without any impurity phase. However, γ-Fe_2O_3 has the same crystal structure and a lattice spacing as Fe_3O_4. To distinguish Fe_3O_4 from γ-Fe_2O_3, the d value of lattice spacing of (311) was calculated by Bragg's equation. The d-spacing value (311) of Fe_3O_4 was calculated to be 2.5249 Å, similar to the value of 2.52516 Å (standard cubic Fe_3O_4: 01-088-0315). As reported by Iida et al. [18], the standard d-spacing value (311) of γ-Fe_2O_3 is 2.5177 Å (γ-Fe_2O_3, JCPDS: 00-039-1346). It can infer that the phase of the obtained material is completely matched with the phase of the standard cubic Fe_3O_4.

Moreover, TPR_{CO} profiles of synthesized Fe_3O_4 further proved that the obtained material was pure Fe_3O_4. As shown in Figure 2, TPR_{CO} profiles illustrated two distinct peaks of the reduction process, corresponding to two-step reduction of $Fe_3O_4 \longrightarrow FeO$ and $FeO \longrightarrow Fe$. There was no peak of the $Fe_2O_3 \longrightarrow Fe_3O_4$ reduction process, referring that there was no presence of Fe_2O_3 in the synthesized material. The reduction temperature of the two-step reduction was approximately 285°C ($Fe_3O_4 \longrightarrow FeO$) and 595°C ($FeO \longrightarrow Fe$). These reduction reactions can be described as follows [19–21]:

$$\begin{aligned} Fe_3O_4 + CO &\longrightarrow 3FeO + CO_2 \\ FeO + CO &\longrightarrow Fe + CO_2 \end{aligned} \quad (1)$$

According to these reports [19–21], the reduction of Fe_3O_4 by carbon monoxide starts in the temperature range of ~509–807°C, which was higher than the reduction temperature of Fe_3O_4 in our study. The lower reaction temperature can be explained due to nanometer-sized Fe_3O_4, reacting with carbon monoxide more easily than crystalline Fe_3O_4.

The morphology of Fe_3O_4 was observed using FE-SEM. As shown in Figure 3(a), Fe_3O_4 exhibited a uniform granular shape with nanoparticles interconnected to each other. The Fe_3O_4 nanoparticles have a diameter of ~10 nm. Besides, the

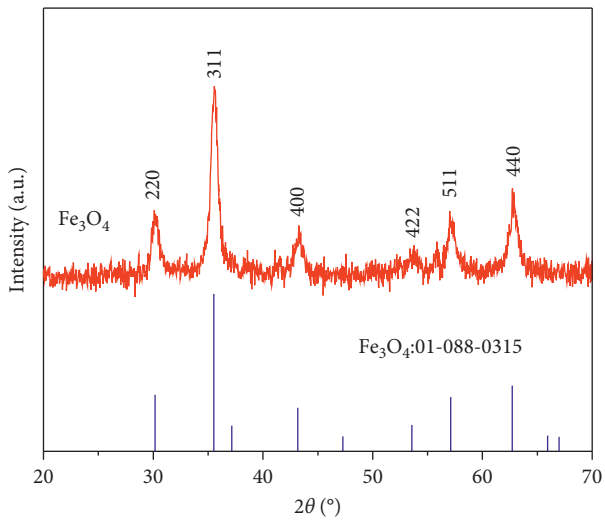

FIGURE 1: XRD patterns of synthesized Fe_3O_4 nanoparticles.

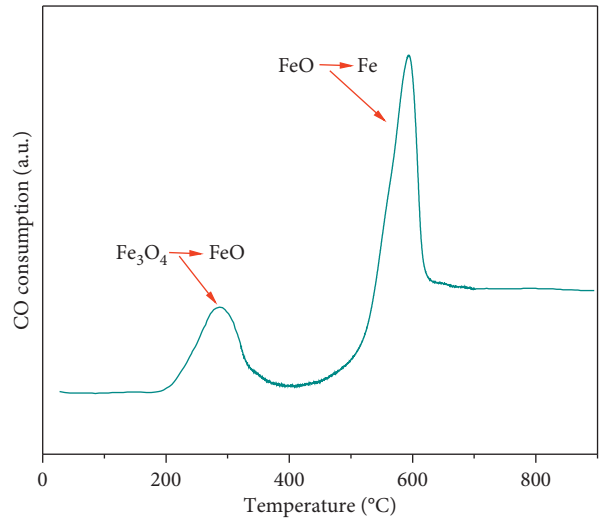

FIGURE 2: TPR_{CO} profile for Fe_3O_4 nanoparticles, a heating rate of 5°C/min.

interconnected Fe_3O_4 nanoparticles formed void spaces which intercalated among Fe_3O_4 nanoparticles as a porous structure. This unique structure plays an important role: it enables better the access of toxic gases to the inside of material, which can improve the adsorption capacity of materials [22]. Furthermore, using Scherrer's equation, the size of Fe_3O_4 particles was calculated to be ~9.8 nm based on the XRD results (Figure 1), suggesting the similar results between XRD and FE-SEM measurement. Figure 3(b) further affirmed the uniform of Fe_3O_4 nanoparticles with the narrow particle-size distribution and the nanosize of Fe_3O_4 [23]. The particle-size distribution of Fe_3O_4 changes from 7 to 13 nm, revealing the good uniform of Fe_3O_4 nanoparticles. The nanometer-sized Fe_3O_4 was expecting to achieve a high specific area. The porous structure of Fe_3O_4 was characterized using N_2 adsorption-desorption isotherms. As shown in Figure 3(c), isotherm adsorption of Fe_3O_4 depicted typical type-IV (multilayer adsorption) that has a broad range of pore sizes and the Barrett–Joyner–Halenda (BJH) pore size distribution (inset) of the Fe_3O_4. Via BET and BJH analysis, the specific area, average pore diameter, and pore volume of Fe_3O_4 were determined to be approximately 115.90 m^2/g, 10.63 nm, and 0.30 cm^3/g, respectively. The relatively high pore size of the Fe_3O_4 particles allow the access of toxic gases inside materials easily. Moreover, the large surface area can facilitate the adsorption of stack gases at the material surface/gases interface [24]. The TGA has proceeded in an air atmosphere with a heating rate of 5°C/min from room temperature to 700°C to evaluate the purity of Fe_3O_4 materials again, as shown in Figure 3(d). The weight gain near 100°C was attributed to the oxidation of Fe_3O_4 to γ-Fe_2O_3. Interestingly, the oxidation temperature in our study is lower than the previous study [25]. This behaviour might be due to the high surface area of the nanometer-sized Fe_3O_4, making them react with oxygen more easily than crystalline Fe_3O_4. Nevertheless, the temperature near 100°C was also the evaporation temperature of moisture from the sample. Because the loss weight owing to the removal of moisture was lower than the weight gain due to the oxidation, the mass change in TG data just shows the mass gain. The content of moisture and Fe_3O_4 in the obtained sample was estimated to be 2.21 and 97.79%, respectively (Figure 3(d)).

3.2. Adsorption Ability of Fe_3O_4 Nanoparticles. Figure 4 shows the adsorption abilities of Fe_3O_4 after exposing to NO_2 in conditions of the study. As shown in Figure 4(a), the intensities of the IR features after 15 minutes exposure to NO_2 start to change, suggesting that the amount of NO_2 was adsorbed on the surface of Fe_3O_4. The adsorption of NO_2 at room temperature leads to an intensity increase of the 1386 cm^{-1} band, corresponding to the band of nitrate (NO_3^-) [26]. The adsorption mechanism of NO_2 on the Fe_3O_4 surface was reported by Eltouny et al. [27] via the following equations:

$$\begin{aligned}
2NO_2\,(\text{gas}) &\longrightarrow 2NO_2\,(\text{adsorbed})\\
2e^- + 2NO_2\,(\text{adsorbed}) &\longrightarrow 2NO_2^-\,(\text{adsorbed})\\
NO_2^-\,(\text{adsorbed}) + NO_2^-\,(\text{adsorbed}) &\longrightarrow NO_3^-\,(\text{adsorbed})\\
&\quad + NO\,(\text{gas}) + e^-\\
NO_2^-\,(\text{adsorbed}) + NO_2\,(\text{gas}) &\longrightarrow NO_3^-\,(\text{adsorbed})\\
&\quad + NO\,(\text{gas})
\end{aligned} \tag{2}$$

The intensity of this peak increases as the time exposing to NO_2 gas increases, suggesting that the larger amount of NO_2 was adsorbed. The uptake of NO_2 by the Fe_3O_4 nanoparticles was shown in Figure 4(b). The amount of NO_2 adsorbed by the Fe_3O_4 reached the saturation level after 60 minutes of exposure. The mass of NO_2 adsorbed by the Fe_3O_4 after 60 minutes of exposure was recorded at 108.5 mg/g of Fe_3O_4. The high adsorption values of the Fe_3O_4 sample were owing to its larger pore volume and high surface area. Furthermore, the presence and mass of NO_2 in the Fe_3O_4 sample were also measured by SEM-EDX

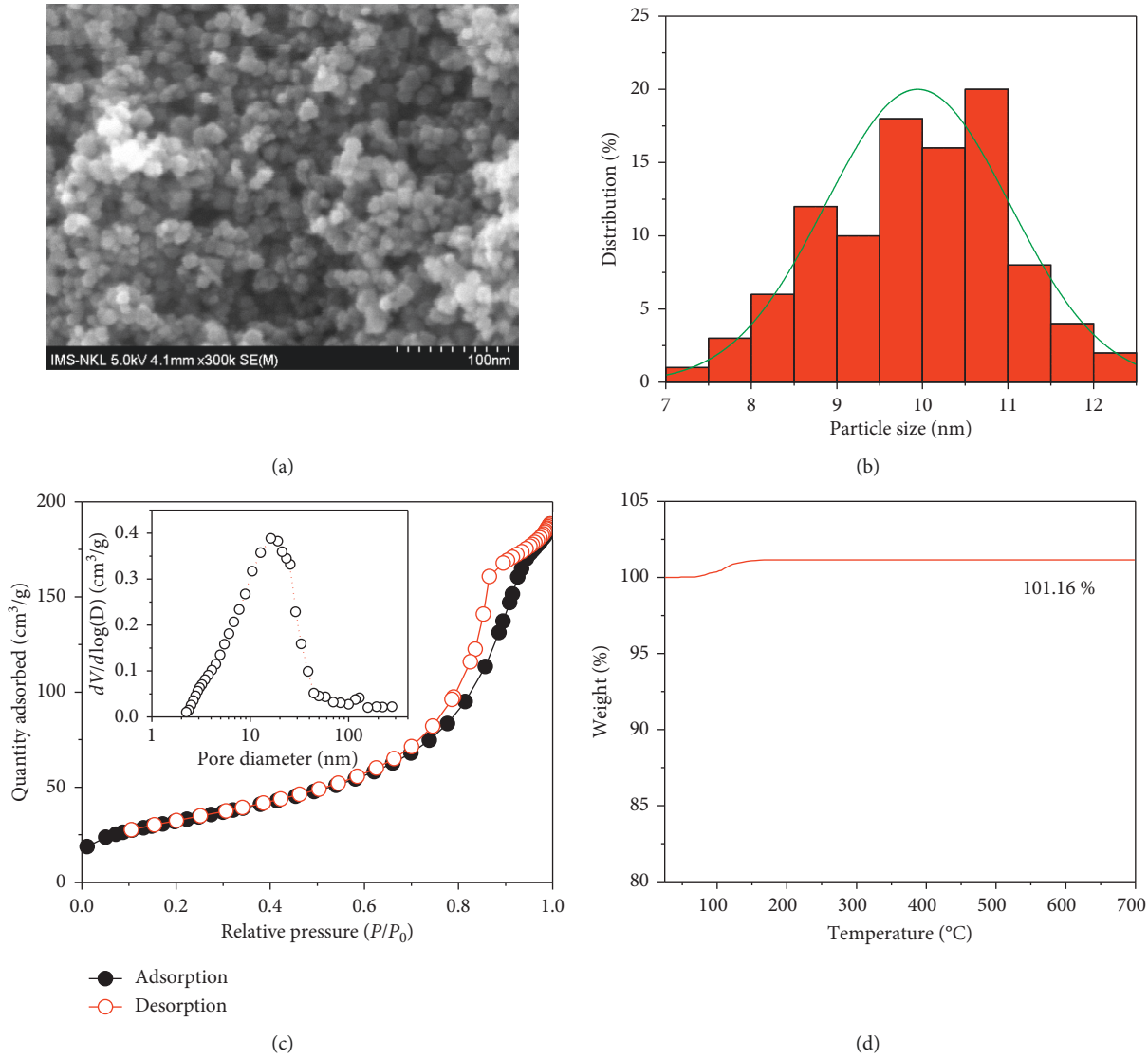

Figure 3: (a) FE-SEM image; (b) particle-size distribution; (c) N_2 adsorption/desorption isotherms; (d) thermogravimetric analysis (TGA) of synthesized Fe_3O_4. Inset in Figure 3(c) shows the pore size distribution calculated from the Barrett–Joyner–Halenda (BJH) formula of synthesized Fe_3O_4.

analysis. As shown in Figure 4(c), the signal of N, Fe, and O elements was detected in the Fe_3O_4 sample exposing to NO_2 after 60 minutes. Based on the intensity of the N element in the sample, %wt. NO_2 in the sample can be, respectively, calculated to be ~9.79 %wt., corresponding to the NO_2 adsorption of ~108.6 mg/g of Fe_3O_4. This result was similar to the adsorption mass of NO_2 by the Fe_3O_4 in Figure 4(b). The morphology of the Fe_3O_4 sample after 60 minutes of exposure to NO_2 was analyzed using the FE-SEM measurement. There was no change in the morphology of Fe_3O_4 nanoparticles before (Figure 3(a)) and after (Figure 4(d)) exposing to the NO_2 gas environment, referring to the stable structure of the Fe_3O_4 sample. Furthermore, the XRD pattern of Fe_3O_4 after exposing with NO_2 (Figure 4(b) inset) did not show any change, compared with the XRD pattern of Fe_3O_4 (Figure 1). The good stable structure can retain the adsorption ability after the regeneration and repeating the NO_2/Fe_3O_4 adsorption many times.

The adsorption abilities of Fe_3O_4 were further examined with the SO_2 gas. Figure 5 shows the adsorption ability of Fe_3O_4 with SO_2. Figure 5(a) shows the FTIR spectra obtained after exposing the Fe_3O_4 sample to SO_2 at different times. The signal at the band of ~1400 and ~1120 cm^{-1}, corresponding to the species of physical adsorption of SO_2, was detected [15]. However, the intensities of SO_2 species were low, suggesting that the small amount of SO_2 was adsorbed on the surface of the Fe_3O_4 sample. The adsorbed amount of SO_2 was displayed in Figure 5(b). The mass of SO_2 adsorbed by the Fe_3O_4 was recorded to 40.5 mg/g of Fe_3O_4 at the saturation level after 60 minutes of exposure. Moreover, the presence and the adsorption mass of SO_2 in the Fe_3O_4 sample was evaluated by SEM-EDX analysis (Figure 5(c)). The signal of the S element was found to be

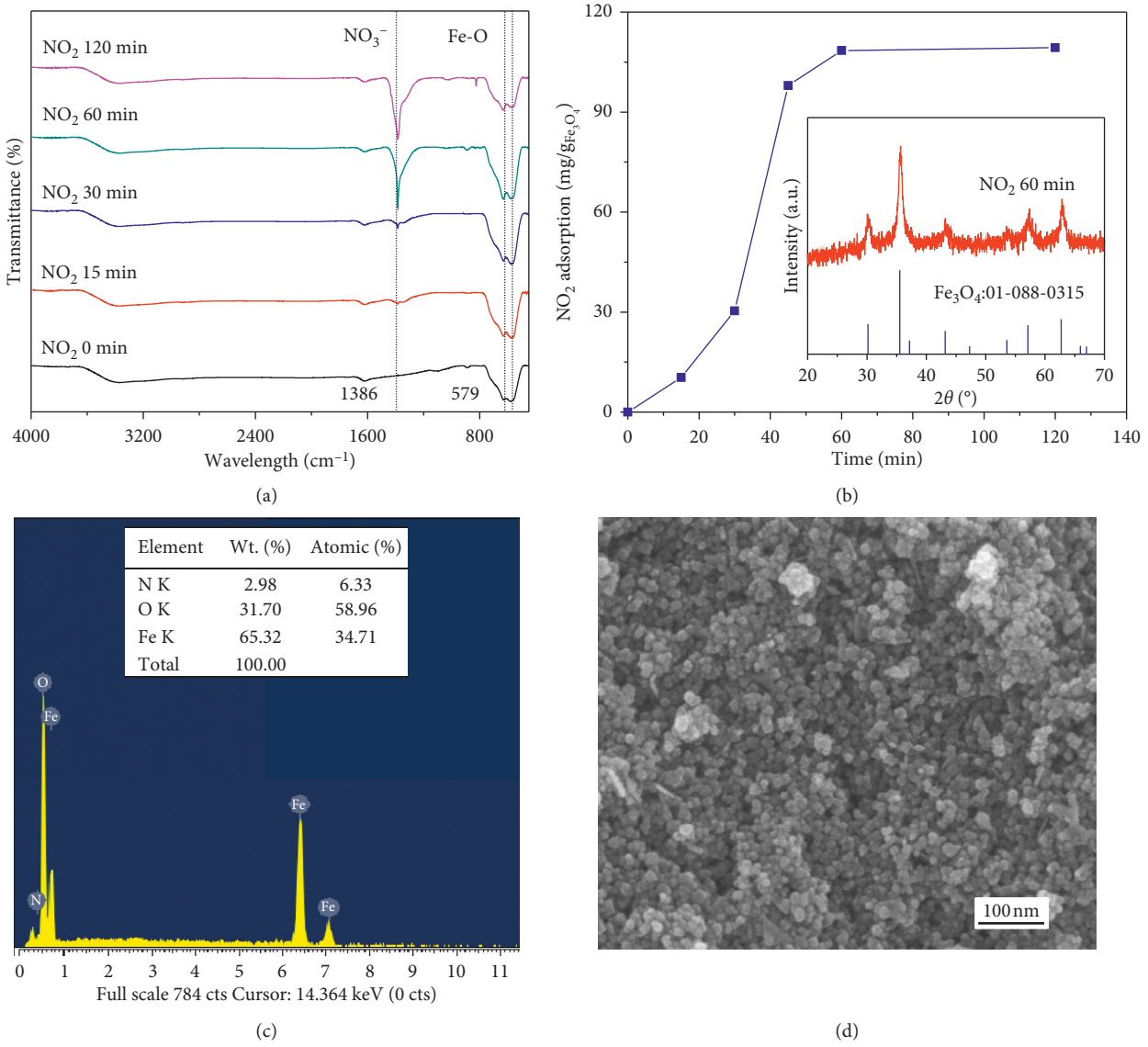

Figure 4: (a) FTIR of Fe_3O_4 samples after exposing to NO_2 gas at the particular time; (b) NO_2 adsorption on Fe_3O_4 samples; (c) SEM-EDX spectra; (d) FE-SEM image of Fe_3O_4 after 60 min of exposure to NO_2. Inset in Figure 4(b) shows the XRD pattern of Fe_3O_4 after 60 min of exposure to NO_2.

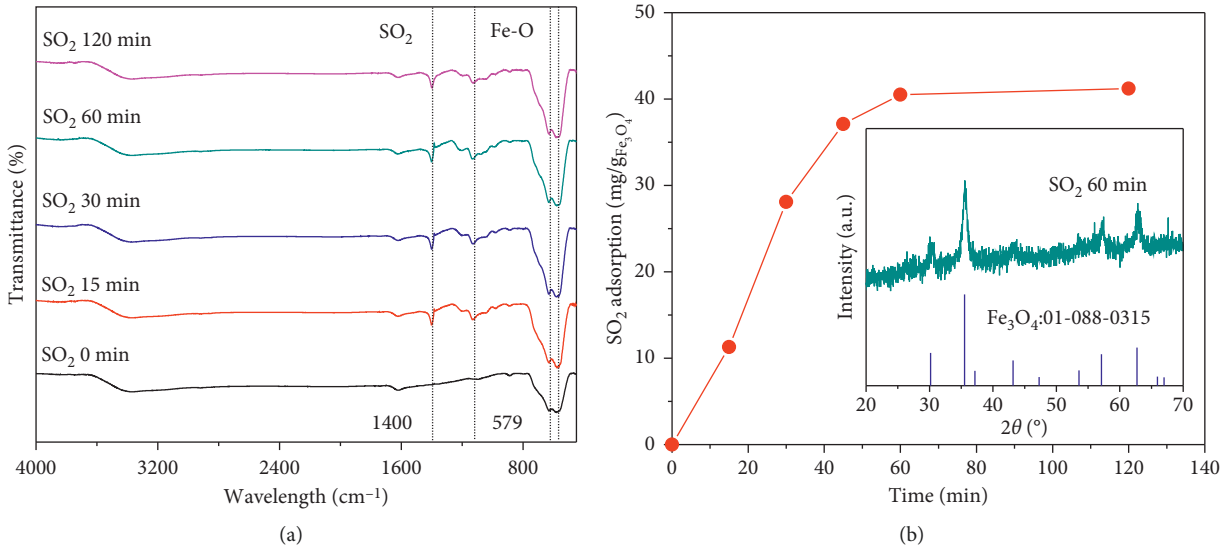

Figure 5: Continued.

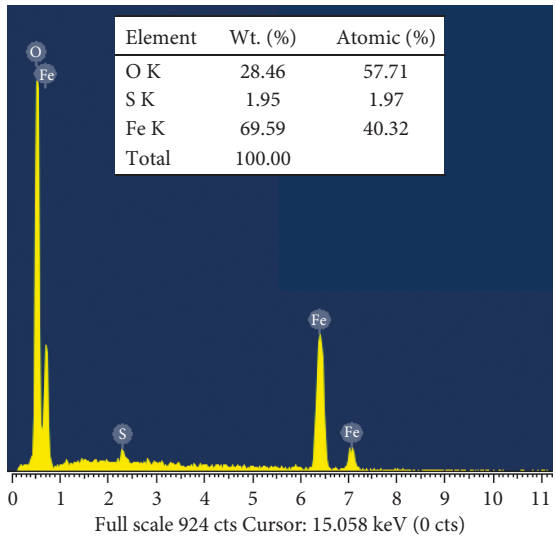

(c)

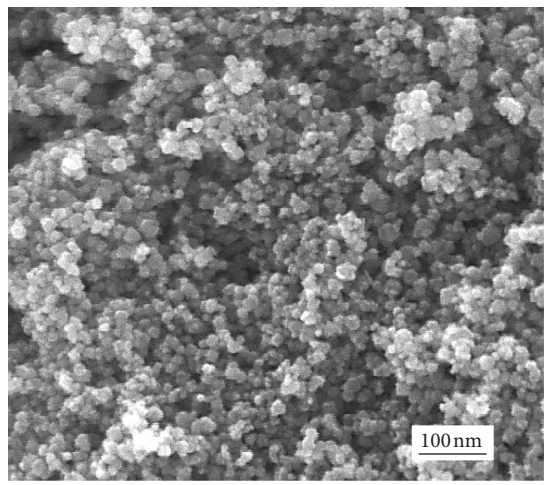

(d)

Figure 5: (a) FTIR of Fe_3O_4 samples after exposing to SO_2 gas at the particular time; (b) SO_2 adsorption on Fe_3O_4 samples; (c) SEM-EDX spectra; (d) FE-SEM image of Fe_3O_4 after 60 min of exposure to SO_2. Inset in Figure 5(b) shows the XRD pattern of Fe_3O_4 after 60 min of exposure to SO_2.

1.95 %wt. of SO_2 in the sample, corresponding to 3.90 SO_2 %wt. in the sample after 60 minutes of exposure. This quantity was calculated to ~40.6 mg/g of Fe_3O_4, similar to the obtained adsorption of Fe_3O_4 in Figure 5(b). The surface of the Fe_3O_4 sample after 60 minutes of exposure with SO_2 was analyzed using FE-SEM measurement. As shown in Figure 5(d), the highly porous structure of Fe_3O_4 was sustained, and no significant change was realized (compared with Figure 3(a)). Moreover, the phase state of Fe_3O_4 (Figure 5(b) inset) after the adsorption also remains, demonstrating the stable-phase state and porous structure. This structure was promising to be recycled and continuously adsorbs gases many times.

4. Conclusions

Fe_3O_4 nanoparticles have successfully been synthesized via the facile scalable method, in which Fe_3O_4 nanoparticles well achieved a porous structure with the high specific area and purity. The Fe_3O_4 nanoparticles exhibited good adsorption with toxic gases. The surface of the Fe_3O_4 nanoparticles adsorbed high amounts of SO_2 and NO_2 of 40.5 mg/g of Fe_3O_4 and 108.5 mg/g of Fe_3O_4, respectively, at a saturation state after 60 minutes of exposure. The high adsorption performance was attributed to the high porosity and specific areas, which enabled the better diffusion and adsorption of toxic gases to the surface of the porous material. The resultant structure of Fe_3O_4 after exposing to the toxic gases would be the good adsorbent, which can be regenerated and adsorb gases many times.

Data Availability

The data used to support the findings of this study are available from the corresponding author upon request.

Conflicts of Interest

The authors declare that there are no conflicts of interest.

Authors' Contributions

Xuan-Manh Pham and Duy Linh Pham contributed equally to this work.

Acknowledgments

This research was funded by Vietnam Academy of Science and Technology under grant number "TĐPCCC.01/18-20."

References

[1] S. Doroudiani, B. Doroudiani, and Z. Doroudiani, "9-Materials that release toxic fumes during fire," in *Toxicity of Building Materials*, F. Pacheco-Torgal, S. Jalali, and A. Fucic, Eds., pp. 241–282, Woodhead Publishing, Cambridge, UK, 2012.

[2] J. Terrill, R. Montgomery, and C. Reinhardt, "Toxic gases from fires," *Science*, vol. 200, no. 4348, pp. 1343–1347, 1978.

[3] W. D. Woolley and M. M. Raftery, "Smoke and toxicity hazards of plastics in fires," *Journal of Hazardous Materials*, vol. 1, no. 3, pp. 215–222, 1975.

[4] B. Truchot, F. Fouillen, and S. Collet, "An experimental evaluation of toxic gas emissions from vehicle fires," *Fire Safety Journal*, vol. 97, pp. 111–118, 2018.

[5] T. Hatakeyama, E. Aida, T. Yokomori, R. Ohmura, and T. Ueda, "Fire extinction using carbon dioxide hydrate," *Industrial & Engineering Chemistry Research*, vol. 48, no. 8, pp. 4083–4087, 2009.

[6] K.-Y. Li, S.-Y. Tsai, C.-P. Lin, Y.-T. Tsai, and C.-M. Shu, "Smart Technology for evaluating fire extinguishing effect of tert-butyl hydroperoxide," *Industrial and Engineering Chemistry Research*, vol. 52, no. 32, pp. 10969–10976, 2013.

[7] S. E. Hunter, L. Li, D. Dierdorf, and T. Armendinger, "Improving water spray efficacy for fire suppression via CO2Addition at high pressures and low temperatures: evidence for CO2Clathrate hydrate formation," *Industrial and Engineering Chemistry Research*, vol. 45, no. 21, pp. 7275–7286, 2006.

[8] J.-M. Hsu, M.-S. Su, C.-Y. Huang, and Y.-S. Duh, "Calorimetric studies and lessons on fires and explosions of a chemical plant producing CHP and DCPO," *Journal of Hazardous Materials*, vol. 217-218, pp. 19–28, 2012.

[9] Y. Lu, J. Yu, and S. Cheng, "Magnetic composite of Fe3O4 and activated carbon as a adsorbent for separation of trace Sr(II) from radioactive wastewater," *Journal of Radioanalytical and Nuclear Chemistry*, vol. 303, no. 3, pp. 2371–2377, 2015.

[10] A. A. Mohammed and I. a. S. Samaka, "Bentonite coated with magnetite Fe 3 O 4 nanoparticles as a novel adsorbent for copper (II) ions removal from water/wastewater," *Environmental Technology and Innovation*, vol. 10, pp. 162–174, 2018.

[11] S. L. Iconaru, R. Guégan, C. L. Popa, M. Motelica-Heino, C. S. Ciobanu, and D. Predoi, "Magnetite (Fe3O4) nanoparticles as adsorbents for as and Cu removal," *Applied Clay Science*, vol. 134, pp. 128–135, 2016.

[12] L. Chai, Y. Wang, N. Zhao, W. Yang, and X. You, "Sulfate-doped Fe3O4/Al2O3 nanoparticles as a novel adsorbent for fluoride removal from drinking water," *Water Research*, vol. 47, no. 12, pp. 4040–4049, 2013.

[13] J. N. Armor, "Catalytic solutions to reduce pollutants," *Catalysis Today*, vol. 38, no. 2, pp. 163–167, 1997.

[14] E. Raymundo-Piñero, D. Cazorla-Amorós, and A. Linares-Solano, "Temperature programmed desorption study on the mechanism of SO2 oxidation by activated carbon and activated carbon fibres," *Carbon*, vol. 39, no. 2, pp. 231–242, 2001.

[15] J. Zawadzki and M. Wiśniewski, "An infrared study of the behavior of SO2 and NOx over carbon and carbon-supported catalysts," *Catalysis Today*, vol. 119, no. 1-4, pp. 213–218, 2007.

[16] M. R. Ghazanfari, M. Kashefi, S. F. Shams, and M. R. Jaafari, "Perspective of Fe_3O_4 nanoparticles role in biomedical applications," *Biochemistry Research International*, vol. 2016, Article ID 7840161, 32 pages, 2016.

[17] S. Wu, A. Sun, F. Zhai et al., "Fe3O4 magnetic nanoparticles synthesis from tailings by ultrasonic chemical co-precipitation," *Materials Letters*, vol. 65, no. 12, pp. 1882–1884, 2011.

[18] H. Iida, K. Takayanagi, T. Nakanishi, and T. Osaka, "Synthesis of Fe3O4 nanoparticles with various sizes and magnetic properties by controlled hydrolysis," *Journal of Colloid and Interface Science*, vol. 314, no. 1, pp. 274–280, 2007.

[19] W. K. Jozwiak, E. Kaczmarek, T. P. Maniecki, W. Ignaczak, and W. Maniukiewicz, "Reduction behavior of iron oxides in hydrogen and carbon monoxide atmospheres," *Applied Catalysis A: General*, vol. 326, no. 1, pp. 17–27, 2007.

[20] B. Hou, H. Zhang, H. Li, and Q. Zhu, "Determination of the intrinsic kinetics of iron oxide reduced by carbon monoxide in an isothermal differential micro-packed bed," *Chinese Journal of Chemical Engineering*, vol. 23, no. 6, pp. 974–980, 2015.

[21] T. S. T. Saharuddin, F. Salleh, A. Samsuri, R. Othaman, and M. A. Yarmo, "Influence of noble metal (Ru, Os and Ag) on the reduction behaviour of iron oxide using carbon monoxide: TPR and kinetic studies," *International Journal of Chemical Engineering and Applications*, vol. 6, no. 6, pp. 405–409, 2015.

[22] T. Jiao, L. Balan, X. Chen, and Q. Zhang, "Functionalized nanocomposites for environmental applications 2015," *Journal of Chemistry*, vol. 2015, Article ID 793265, 1 pages, 2015.

[23] H. Meng, Z. Zhang, F. Zhao, T. Qiu, and J. Yang, "Orthogonal optimization design for preparation of Fe3O4 nanoparticles via chemical coprecipitation," *Applied Surface Science*, vol. 280, pp. 679–685, 2013.

[24] T. Jiao, X. Yan, L. Balan, A. L. Stepanov, X. Chen, and M. Z. Hu, "Chemical functionalization, self-assembly, and applications of nanomaterials and nanocomposites," *Journal of Nanomaterials*, vol. 2014, Article ID 291013, 2 pages, 2014.

[25] I. Kazeminezhad and S. Mosivand, "Phase transition of electrooxidized Fe3O4 to gamma and alpha-Fe2O3 nanoparticles using sintering treatment," *Acta Physica Polonica Series A*, vol. 125, no. 5, pp. 1210–1214, 2014.

[26] C. Sedlmair, B. Gil, K. Seshan, A. Jentys, and J. A. Lercher, "An in situ IR study of the NOx adsorption/reduction mechanism on modified Y zeolites," *Physical Chemistry Chemical Physics*, vol. 5, no. 9, pp. 1897–1905, 2003.

[27] N. Eltouny and P. A. Ariya, "Competing reactions of selected atmospheric gases on Fe3O4nanoparticles surfaces," *Physical Chemistry Chemical Physics*, vol. 16, no. 42, pp. 23056–23066, 2014.